ACS APPLIED MATERIALS & INTERFACES

Research Article

Cite This: ACS Appl. Mater. Interfaces 2018, 10, 22552−22561

www.acsami.org

# Distinct Photovoltaic Performance of Hierarchical Nanostructures Self-Assembled from Multiblock Copolymers

Zhanwen Xu,[†] Jiaping Lin,*[,†] Liangshun Zhang,[†] Liquan Wang,*[,†] Gengchao Wang,[†] Xiaohui Tian,[†] and Tao Jiang[‡]

[†]Shanghai Key Laboratory of Advanced Polymeric Materials, Key Laboratory for Ultrafine Materials of Ministry of Education, State Key Laboratory of Bioreactor Engineering, School of Materials Science and Engineering, East China University of Science and Technology, Shanghai 200237, China

[‡]Beijing Institute of Nanoenergy and Nanosystems, Chinese Academy of Sciences, Beijing 100083, China

Supporting Information

**ABSTRACT:** We applied a multiscale approach coupling dissipative particle dynamics method with a drift-diffusion model to elucidate the photovoltaic properties of multiblock copolymers consisting of alternating electron donor and acceptor blocks. A series of hierarchical lamellae-in-lamellar structures were obtained from the self-assembly of the multiblock copolymers. A distinct improvement in photovoltaic performance upon the morphology transformation from lamella to lamellae-in-lamella was observed. The hierarchical lamellae-in-lamellar structures significantly enhanced exciton dissociation and charge carrier transport, which consequently contributed to the improved photovoltaic performance. On the basis of our theoretical calculations, the hierarchical nanostructures can achieve much enhanced energy conversion efficiencies, improved by around 25% compared with that of general ones, through structure modulation on the number and size of the small-length-scale domains via the molecular design of multiblock copolymers. Our findings are supported by recent experimental evidence and provide guidance for designing advanced photovoltaic materials with hierarchical structures.

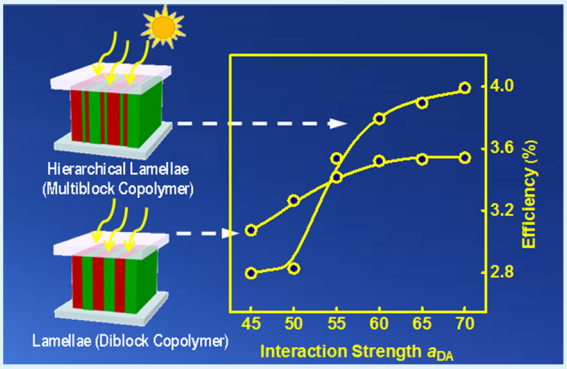


**KEYWORDS:** *hierarchical nanostructures, photovoltaic devices, polymer solar cells, lamellae-in-lamellar structures*

## 1. INTRODUCTION

Polymer photovoltaic devices, which offer many advantages, such as low cost, high mechanical flexibility, lightweight, and large-area manufacturing compatibility at relatively low processing temperatures, have received increasing attention.[1−3] Lightweight, flexible polymer photovoltaics are better suited for portable power applications and would open more market opportunities than inorganic photovoltaic cells such as silicon cells. However, the lower power conversion efficiencies ($\eta$) of polymer photovoltaics limit their commercialization.[4] Research efforts in the last decade have significantly improved the polymer solar cell performance.[5−8] Despite some breakthroughs, however, the efficiencies required to compete in the energy market have not yet been realized. It is worth noting that block copolymer-based polymer solar cells, which are very promising, have shown stubbornly low efficiencies of ∼3%.[9,10] Enhancing the photovoltaic performance of polymer solar cells presents a pressing challenge.

Typical polymer solar cells consist of a polymer donor (electron-transporting) and an acceptor (hole-transporting) as the photoactive layer. The morphology of the active layer is a key factor for high performance.[11,12] Optimizing the morphology can enhance the exciton dissociation (charge carrier generation) at the donor/acceptor (D/A) interface, improve charge transport, and maximize the collection of the dissociated electrons and holes at the electrodes. Various structures, such as ordered continuous networks, lamellar, and cylindrical structures, have been applied to optimize the morphology.[13−16] Among these structures, hierarchical nanostructures with different length scales have recently been reported to possess improved photovoltaic properties.[17−20] Chen et al. have fabricated PTB7/fullerene photovoltaic devices harboring hierarchical nanostructures ranging from several nanometers of crystallites to tens of nanometers of nanocrystallite aggregates in PTB7-rich and fullerene-rich domains.[17] These devices exhibit superior performance, which is attributed to the significantly enhanced exciton dissociation resulting from the hierarchical morphologies. Very recently, Fang et al. have achieved hierarchical phase separation in ternary polymer blend solar cells.[20] Their results indicated that devices with hierarchical structures show improved photovoltaic performance. Because the hierarchical

Received: March 22, 2018
Accepted: June 14, 2018
Published: June 14, 2018






DOI: 10.1021/acsami.8b04692
ACS Appl. Mater. Interfaces 2018, 10, 22552−22561

structures formed in polymer blends are usually dynamically trapped, disarranged, and uncontrollable,[21,22] it is a great challenge to optimize morphologies for higher photovoltaic performance in blend systems. Controlling the structural hierarchy is vital for correlating photovoltaic performance with hierarchical structures and further optimizing the structures to obtain outstanding performance for polymer solar cells.

In contrast with polymer blends, multiblock copolymers can self-assemble into hierarchically ordered nanostructures with thermodynamic stability. So far, a number of works have reported the preparation of hierarchical structures through the self-assembly of multiblock copolymers.[23−26] For example, ten Brinke et al. have obtained a hierarchical lamellae-in-lamellar structure from the self-assembly of two-length-scale A-*b*-(B-*b*-A)$_n$-*b*-B multiblock copolymers.[27] We also predicted a series of hierarchical structures, including cylinders-in-lamellae, lamellae-in-lamellae, cylinders-in-cylinders, and spheres-in-spheres, in A(BC)$_n$ multiblock copolymers via using self-consistent field theory.[28,29] Additionally, we have shown that hierarchical nanostructures exhibited excellent properties such as distinct elastic response.[30] So far, most of the multiblock copolymers investigated in these studies are flexible. However, the multiblock copolymers used in photovoltaic devices should contain conjugated polymers (semiconductor polymers), which are usually rigid.[22,31,32] Recently, Hiorns et al. successfully synthesized a conjugated donor−acceptor multiblock copolymer that could be applied in polymer solar cells.[33] They incorporated a high-fullerene-content polymer with poly(3-hexylthiophene) into a multiblock copolymer. Ordered lamellar structures have been obtained in these conjugated multiblock copolymers. These works suggest that hierarchically ordered structures for application in polymer solar cells can be obtained through the self-assembly of donor−acceptor (DA) conjugated multiblock copolymers with blocks of different length scales. However, the question remains whether the solar cells with hierarchically ordered structures formed by DA multiblock copolymers can have improved photovoltaic performance. The correlation between the photovoltaic performance and the hierarchical nanostructures of multiblock copolymers should be examined to address this question.

Theoretical simulations have been used to examine the relationship between the nanostructures and the photovoltaic properties.[34−37] Two computational methods are generally used to address this issue: kinetic Monte Carlo (KMC) method and drift-diffusion model.[38,39] For example, Kimber et al. applied the KMC method to study the photovoltaic performances of a series of morphologies including bicontinuous nanostructures and cylindrical nanostructures, which are potential structures for polymer solar cells.[16] Their simulations predicted that the cylindrical nanostructures perform much better than the blend morphologies and bicontinuous nanostructures. This is a good example showing the predictive power of the KMC method in the field of polymer solar cells. However, the KMC method requires high computation cost. As an alternative method, the drift-diffusion method is significantly faster than the KMC method in accomplishing a single current−voltage sweep.[38,40] The fast current−voltage sweep enables the research studies on the photovoltaic performance of complex hierarchical nanostructures. On the basis of the drift-diffusion simulations, Koster et al. successfully reproduced the $J-V$ curves in experiments and established a quantitative link between the efficiency and the three-dimensional blend morphology.[40] In the above works, the morphologies are usually designed or constructed artificially. Unlike these works, we aim to use a simulation method, dissipative particle dynamics (DPD), to predict the nanostructures self-assembled from a series of multiblock copolymers with complex architectures. (Note that in the DPD simulations, the nature of the complex polymer can be well described.) Then, we apply the drift-diffusion model to calculate photovoltaic properties of the nanostructures self-assembled from the multiblock copolymers.

In this work, to the best of our knowledge, we report a first investigation of the photovoltaic properties of DA multiblock copolymers consisting of alternating short and long blocks. A multiscale approach involving morphological studies with DPD and calculations of photovoltaic properties via solving drift-diffusion equations is employed to study the self-assembled nanostructures and the corresponding photovoltaic properties. A series of ordered hierarchical nanostructures self-assembled from the DA multiblock copolymers were predicted through the DPD simulations. The calculations of photovoltaic properties demonstrate that an improvement in photovoltaic performance can be obtained by a change in morphology from general nanostructures to hierarchical nanostructures. We expect this work to provide useful information for designing advanced photovoltaic materials with hierarchical structures.

## 2. RESULTS AND DISCUSSION

In this work, we investigated the relation between the hierarchical nanostructures and the photovoltaic properties of D′(AD)$_n$A′ multiblock copolymers. The multiblock copolymers consist of long outer blocks and short inner blocks, as shown in Figure 1a. In the simulations, the volume fraction of donor blocks was set to 0.5, and the ratio of donors to acceptors was thus 1:1. Two important parameters influencing the self-assembled nanostructures of the D′(AD)$_n$A′ copolymers were considered: the number of the repeat AD units

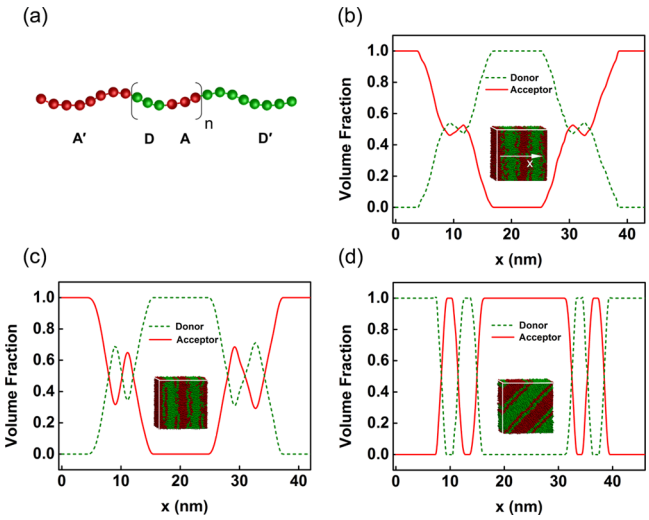


**Figure 1.** (a) Molecular architectures of D′(AD)$_n$A′ multiblock copolymers. (b−d) One-dimensional density profiles of acceptor (red solid line) and donor (green dashed line) blocks of D′(AD)$_n$A′ multiblock copolymers along the *x*-direction vertical to the donor−acceptor interface at various $a_{DA}$ values: (b) $a_{DA}$ = 45, (c) $a_{DA}$ = 55, and (d) $a_{DA}$ = 70. The insets show the corresponding three-dimensional nanostructures.



DOI: 10.1021/acsami.8b04692
ACS Appl. Mater. Interfaces 2018, 10, 22552−22561

governing the number of small domains and the length of the short inner blocks controlling the size of small domains.

**2.1. Enhanced Photovoltaic Performance in Hierarchical Nanostructures.** In this subsection, we examined the influence of the formation of structural hierarchy on the photovoltaic performance of D′(AD)$_n$A′ multiblock copolymers. The lengths of the short and long blocks were set to 3 and 8, respectively. The number ($n$) of repeat AD midblocks in D′(AD)$_n$A′ was set to 1. The repulsive interaction parameter between D and A beads $a_{DA}$ was varied from 45 to 70. The electrical parameters used in the photovoltaic calculations are listed in Table 1. Most of the parameters are typical for polymeric materials used in polymer photovoltaic cells.[41−44] The exciton lifetime was set to 1 $\mu$s according to the literature.[42,43] The electron and hole mobilities are both set to $10^{-8}$ m$^{-2}$ V$^{-1}$ s$^{-1}$, which is in the magnitude of the charge mobilities of P3HT-*b*-PPCBM block copolymers (the P3HT-*b*-PPCBM incorporating poly(3-hexylthiophene) as the donor and polystyrene with pendant fullerenes as the acceptor block).[40] In the simulations, we assumed that the electronic properties of the multiblock copolymers remained unchanged during the variation of the repulsive parameter $a_{DA}$ because the change in interaction parameters does not significantly alter the permittivity and the charge carrier mobility.[45]

**Table 1. Parameters for the Drift-Diffusion Model**

| parameter | symbol | value |
|---|---|---|
| hole mobility (zero-field) | $\mu_{h0}$ | $10^{-8}$ m$^2$ V$^{-1}$ s$^{-1}$ |
| electron mobility (zero-field) | $\mu_{e0}$ | $10^{-8}$ m$^2$ V$^{-1}$ s$^{-1}$ |
| field-dependent constant for hole mobility | $\gamma_h$ | $2.4 \times 10^{-4}$ m$^{1/2}$ V$^{-1/2}$ |
| field-dependent constant for electron mobility | $\gamma_e$ | $2.4 \times 10^{-4}$ m$^{1/2}$ V$^{-1/2}$ |
| exciton diffusion length | $l_d$ | 10 nm |
| exciton lifetime | $\tau$ | $10^{-6}$ s |
| donor HOMO | HOMOD | 5.2 eV |
| donor LUMO | LUMOD | 3.5 eV |
| acceptor HOMO | HOMOA | 6.1 eV |
| acceptor LUMO | LUMOA | 3.7 eV |
| cathode work function | $\phi_c$ | 3.9 eV |
| anode work function | $\phi_a$ | 4.7 eV |

To understand the relationship between the nanostructures and the photovoltaic properties of the D′(AD)$_1$A′ copolymers, we first examined the effect of $a_{DA}$ on self-assembled nanostructures of the multiblock copolymers. Figure 1b−d shows the one-dimensional density profiles ($\varphi_i$) of the donor and acceptor components along the direction normal to the D/A interface in the self-assembled nanostructures at different degrees of separation. In each figure, the inset is the corresponding three-dimensional nanostructure. These data were collected after the systems reached a steady state, according to the fact that the potential energy and pressure tensor components no longer changed with time.[29] As shown in Figure 1b, weakly segregated lamellae are obtained with $a_{DA}$ = 45. It is obvious from the density profiles that the long D′ blocks and A′ blocks mainly form D-rich ($\varphi_D$ = 1) and A-rich ($\varphi_A$ = 1) lamellar domains, respectively. In addition, the short AD blocks form a mixed layer, where both $\varphi_D$ and $\varphi_A$ are close to 0.5. When $a_{DA}$ increases to 55, the D′(AD)$_1$A′ copolymers form parallel lamellae-in-lamellae with two small domains between every two neighboring large domains (**L**$_2$-in-**L**), as can be seen from Figure 1c. At a higher repulsive parameter $a_{DA}$, strongly separated lamellae-in-lamellae emerge (Figure 1d). The D and A components separated from each other so strongly that the short blocks form pure D and A small domains as reflected by the density profiles.

During the transformation of the general lamellae into lamellae-in-lamellae, the photovoltaic performance changes markedly. Figure 2 shows the $J$−$V$ (current density−applied voltage) curves for the structures self-assembled from the D′(AD)$_1$A′ multiblock copolymers. The $J$−$V$ curves are calculated under applied voltages in the range from 0.0 to 0.7 V using the drift-diffusion model. In addition, the output power, which is the product of current density and applied voltage, was calculated to analyze the energy conversion. Figure 2a,b presents the $J$−$V$ curves and output powers, respectively. The short-current density ($J_{sc}$) and open-circuit voltages ($V_{oc}$) of the $J$−$V$ curves increase as the repulsive parameter $a_{DA}$ increases, as shown in Figure 2a. Figure 2b shows that the maximum output power increases markedly as the $a_{DA}$ value increases.

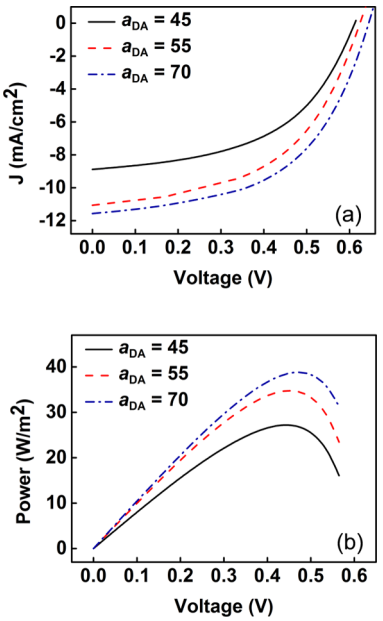


**Figure 2.** $J$−$V$ curves (a) and output powers (b) as a function of applied voltage for systems with hierarchical nanostructures self-assembled from D′(AD)$_1$A′ multiblock copolymers with various $a_{DA}$ values. The thickness of the active layer in these systems is 100 nm.

The photovoltaic properties, including $J_{sc}$, $V_{oc}$, $\eta$, and the fill factor (FF), can be calculated from the $J$−$V$ curves, which are usually applied to characterize photovoltaic devices. The obtained values of $J_{sc}$, $V_{oc}$, $\eta$, and FF as a function of $a_{DA}$ are given in Figure 3. The photovoltaic properties exhibit different responses to the change in $a_{DA}$, with three regions. As can be seen in Figure 3a, in the $a_{DA}$ range of 45−50 (region I), $J_{sc}$ increases slightly with increasing $a_{DA}$. In region I, the multiblock copolymers self-assemble into the general lamellae, as can be seen in Figure 1b. In region II ($a_{DA}$ increases from 50 to 60), $J_{sc}$ increases markedly with the increase in $a_{DA}$, in which the nanostructures undergo the transformation of lamellae into lamellae-in-lamellae (Figure 1c). In region III ($a_{DA}$ is greater than 60), $J_{sc}$ increases slightly with the increase in the value of $a_{DA}$, in which the well-segregated small domains are obtained in the lamellae-in-lamellae (see Figure 1d). Compared with $J_{sc}$,


DOI: 10.1021/acsami.8b04692
ACS Appl. Mater. Interfaces 2018, 10, 22552−22561

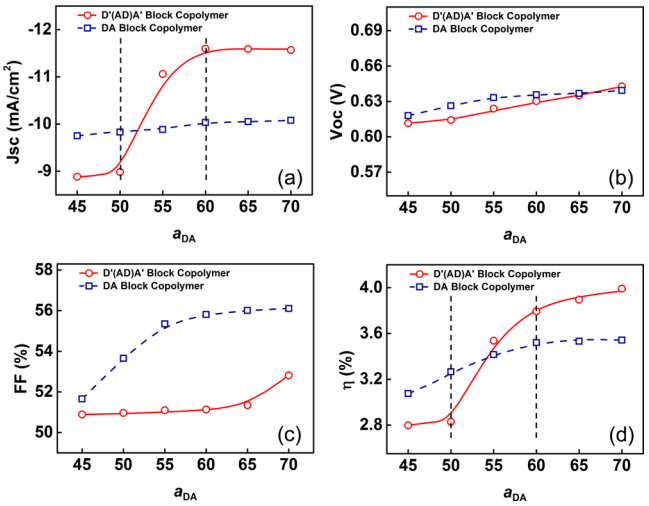


**Figure 3.** Plots of $J_{sc}$ (a), $V_{oc}$ (b), FF (c), and $\eta$ (d) as a function of $a_{DA}$ for D′(AD)$_1$A′ multiblock copolymers and DA diblock copolymers.

the values of $V_{oc}$ and FF are less sensitive to the variation in $a_{DA}$, as shown in Figure 3b,c. The evolution of $\eta$ with increasing $a_{DA}$ is similar to that of $J_{sc}$, as shown in Figure 3d. The value of $\eta$ as a function of $a_{DA}$ also increases greatly in region II, in which the lamellae change to lamellae-in-lamellae. The photovoltaic performance is significantly improved as the lamellae-in-lamellae are formed.

To obtain a deep understanding of the enhancement in the photovoltaic properties of the hierarchical structures, we also calculated the $J_{sc}$, $V_{oc}$, $\eta$, and FF of lamellar structures formed by DA diblock copolymers for a comparison. The adopted block length of the diblock copolymer was the same as that of the long block of the D′(AD)A′ multiblock copolymer. In Figure 3a–d, the blue lines represent the $J_{sc}$, $V_{oc}$, FF, and $\eta$ of the DA diblock copolymer. The photovoltaic properties increase slightly with increasing $a_{DA}$. The $V_{oc}$ of the diblock copolymer is close to that of the multiblock copolymer (Figure 3b). The FF of the diblock copolymer is higher than that of the multiblock copolymer, as shown in Figure 3c. In contrast to $V_{oc}$ and FF, there are significant differences in $J_{sc}$ and $\eta$ between the diblock and multiblock copolymers (see Figure 3a,d). In region I, the photovoltaic properties of the DA diblock copolymer, including $J_{sc}$ and $\eta$, are higher than those of the D′(AD)A′ multiblock copolymer. However, in regions II and III, DA diblock copolymers display slightly increasing $J_{sc}$ and $\eta$, showing much weaker photovoltaic performance than the D′(AD)A′ multiblock copolymer. These results indicate that the D′(AD)A′ multiblock copolymers forming lamellae-in-lamellae show a clear advantage over the DA diblock copolymers in terms of photovoltaic performance. To confirm that lamellae-in-lamellar structures perform better than optimized general lamellar structures, we performed additional photovoltaic calculations on the performance of a series of lamellae-in-lamellar and general lamellar structures with various domain spacings (see Section 3 of the Supporting Information). It was found that the $\eta$ of the optimized general lamellar structure is still lower than that of the lamellae-in-lamellar structures (see Figure S1).

To capture the underlying mechanism of the enhancement of photovoltaic performance generated by the hierarchical nanostructures, we calculated the equilibrium distributions of the exciton concentrations, photogenerated current densities, and charge carrier recombination rates, all of which significantly affect the photovoltaic processes. Figure 4 shows

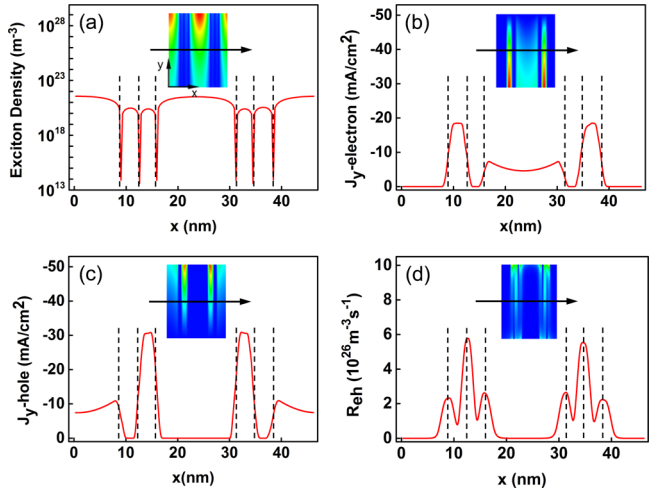


**Figure 4.** Plots of exciton density (a), electron-current density along the $y$-coordinate perpendicular to the electrodes (b), hole-current density along the $y$-coordinate (c), and charge carrier recombination rate (d) as a function of the $x$-coordinate perpendicular to the donor–acceptor interface in the middle of the systems with $\mathbf{L}_2$-in-$\mathbf{L}$ structures. The insets show the two-dimensional distributions. The red and blue regions correspond to high and low values, respectively. The dashed lines in each figure are plotted at the D/A interfaces.

these distributions in the hierarchical lamellae with $a_{DA}$ = 70, where the completely segregated small domains are formed. The inset images show the corresponding two-dimensional distributions. Figure 4a shows the exciton concentrations in $\mathbf{L}_2$-in-$\mathbf{L}$. The exciton concentrations drop to very low values near the D/A interfaces, as excitons dissociate in these regions. Furthermore, the exciton concentrations in the small domains are much lower than those in the large domains, which indicates that more excitons from the small domains than those from the large domains can successfully diffuse to the D/A interfaces and dissociate into free charge carriers. As more excitons in the small domains undergo dissociation, more charge carriers are generated in the small domains, which leads to higher current densities in the small domains. This phenomenon can be observed in Figure 4b,c, which shows the electron-current densities and hole-current densities along the $y$-coordinate, respectively. Both the electron-current densities and hole-current densities in the small domains are higher than those in the large domains. However, the charge carriers in the small domains are more likely to diffuse back to the D/A interfaces and undergo recombination. It is apparent from Figure 4d that the charge carrier recombination rates in the large domains are lower than those in the small domains. From these results, we learned that the small domains in the hierarchical structures enhance exciton dissociation (charge carrier generation), and the large domains are favorable for charge carrier transport and collection with low recombination rates. The enhanced exciton dissociation in small domains and low recombination rates in large domains result in the enhancement of the photovoltaic performance for the hierarchical nanostructures.

It should be noted that the electronic properties of the materials, such as the permittivity and the charge carrier


DOI: 10.1021/acsami.8b04692
ACS Appl. Mater. Interfaces 2018, 10, 22552–22561

mobility, are assumed not to change with impure phases in our model. In fact, the mixed phases can significantly change the properties in some materials and then affect the device performance.[46−49] For example, Sweetnam et al. found that when the phase purity is increased by increasing the molecular interaction, the energy levels are also modulated.[49] The modulated energy levels can aid in spatially separating charge carriers and suppressing bimolecular recombination.[50] According to these facts, we can deduce that if the effect of the mixed phases on energy levels was included in the simulations, the predicted performances of lamellae-in-lamellae and general lamellae could be changed. However, our conclusion, the lamellae-in-lamellae performing better than the lamellae, could be general. We have calculated the photovoltaic properties of the self-assembled nanostructures of block copolymers with the charge carrier mobility increasing from $10^{-8}$ to $10^{-7}$ $m^{-2}$ $V^{-1}$ $s^{-1}$ (see Section 4 of the Supporting Information). Though both the photovoltaic properties of lamellae-in-lamellae and lamellae are changed, the lamellae-in-lamellae still perform better than the lamellae (see Figure S2). Additionally, we have also examined the effect of the change in exciton lifetime on our results (see Section 5 of the Supporting Information). It was found that the change in the exciton lifetime does not affect much our results (see Figure S3).

**2.2. Effect of the Number of Small Domains.** In this subsection, we extend to analyze the photovoltaic performance of **L**-in-**L** structures having various numbers of small domains. In our previous works, it is learned that C′(RC)$_n$R′ rod-coil multiblock copolymers can self-assemble into **L**-in-**L** structures, and the number of small domains can be tuned by changing the number of repeat RC units ($n$).[51] Similar to the hierarchical nanostructures of the rod-coil multiblocks, the number of small domains in the **L**-in-**L** structures formed by the D′(AD)$_n$A′ multiblock copolymers is also tunable. Herein, the number of repeat AD units is varied to modulate the number of small domains.

As described in the above section, D′(AD)$_1$A′ copolymers can self-assemble into hierarchical **L**$_2$-in-**L** structure with two small domains between every two neighboring large domains. In this subsection, to obtain hierarchical structures with more small domains, we consider the self-assembly of D′(AD)$_2$A′ and D′(AD)$_3$A′ copolymers with two and three inner AD units, respectively. In addition, the photovoltaic performance of the nanostructures formed by these copolymers is compared with those of **L**$_2$-in-**L** and general lamellar structures. Figure 5 displays the structures obtained in these two copolymers with repulsive parameter $a_{DA}$ set to 70. Hierarchical **L**-in-**L** structures with controlled numbers of small domains were successfully obtained. The D′(AD)$_2$A′ copolymers self-assemble into a hierarchical structure with four small domains (two donor layers and two acceptor layers) between every two neighboring large domains (**L**$_4$-in-**L**) (Figure 5a). As D′(AD)$_3$A′ has one more AD repeat unit than D′(AD)$_2$A′, two more small domains were formed between every two neighboring large domains (**L**$_6$-in-**L**) (Figure 5b).

Figure 6 displays the photovoltaic properties as a function of the number of small domains in the **L**-in-**L** structures. In this figure, the case with zero small domains corresponds to the general lamellar structure. As shown in Figure 6a, the $V_{oc}$ value remains almost unchanged as the number of small domains increases, whereas $J_{sc}$ increases significantly. In contrast to $J_{sc}$, FF is found to decrease as the number of small domains increases, as shown in Figure 6b. Whereas both $J_{sc}$ and FF

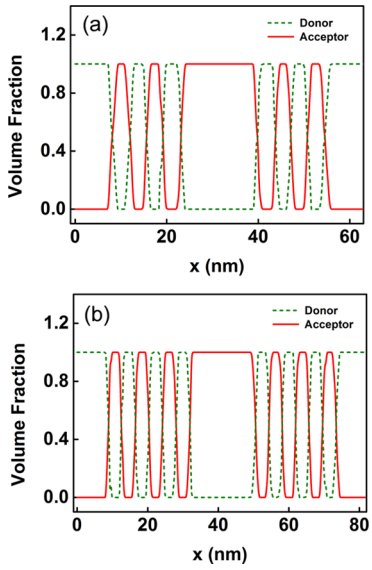


**Figure 5.** One-dimensional density profiles of donor and acceptor blocks along the $x$-direction perpendicular to the donor−acceptor interface of the structures self-assembled from (a) D′(AD)$_2$A′ and (b) D′(AD)$_3$A′ multiblock copolymers.

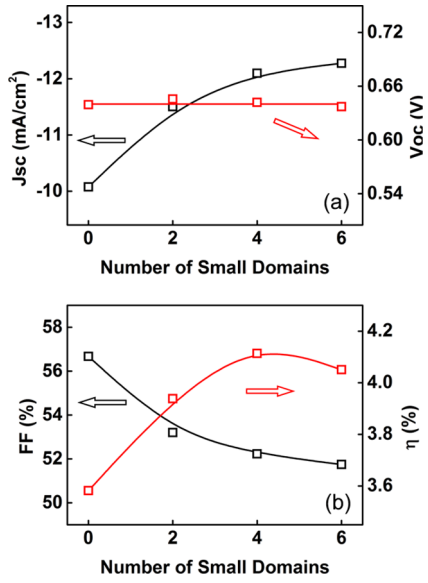


**Figure 6.** Plots of $J_{sc}$ and $V_{oc}$ (a) and FF and $\eta$ (b) as a function of the number of the small domains in the nanostructures self-assembled from D′(AD)$_n$A′ copolymers with n varying from 0 to 3.

show a monotonic dependence on the number of small domains, $\eta$ varies nonmonotonically as a function of the number of small domains. As the number of small domains increases, $\eta$ first increases and then decreases (see Figure 6b). The value of $\eta$ reaches its maximum when the number of small domains is 4. The existence of the optimized number can be attributed to the opposite dependence of $J_{sc}$ and FF on the number of small domains.

The dependence of the photovoltaic properties on the number of small domains can be understood by examining the generation and recombination of charge carriers. Because small domains favor exciton dissociation (see Figure 4a), more small domains can lead to a higher exciton dissociation ratio and thus higher photogenerated current densities (see Figure S4).


DOI: 10.1021/acsami.8b04692
ACS Appl. Mater. Interfaces 2018, 10, 22552−22561

This increase in photogenerated current density results in the monotonic increase of $J_{sc}$ (see Figure 6a). On the other hand, small domains can also lead to higher charge carrier recombination rates (see Figure 4d), resulting in the increase of the charge carrier recombination current density as the number of small domains increases (see Figure S4). The FF is dominated by charge carrier recombination, and stronger recombination leads to a lower FF. As a consequence, the increase in recombination current leads to a decrease in FF as the number of small domains increases (Figure 6b). Because increasing the number of small domains enhances both the generation and recombination of charge carriers, there should be an optimized number of small domains balancing these effects. In our calculations, the hierarchical structure with four small domains showed the highest $\eta$.

**2.3. Effect of Size of Small Domains.** The domain size of the active layer has an important influence on the photovoltaic performance of polymer solar cells. Both experimental and simulation studies have shown that the photovoltaic properties become much more sensitive to domain changes as the domain size decreases.[16,37,52] The photovoltaic performance of the hierarchical structures could depend strongly on the size of the small domains. In this subsection, we examine the influence of the size of the small domains on the photovoltaic performance of the lamellae-in-lamellar structures. For the self-assembly of conjugated block copolymers, the domain size can be controlled by the length of the blocks.[53,54] On the basis of this fact, it can be anticipated that the size of small domains in $D'(AD)_nA'$ multiblock copolymers could be modulated by varying the length (the number of beads, $N$) of the short blocks. Therefore, we conducted a study of the hierarchical nanostructures and the corresponding photovoltaic properties of the $D'_8(A_ND_N)A'_8$ with $N$ varying from 3 to 7.

Figure 7 displays the domain size as a function of the length $N$ of the short blocks with the repulsive parameter $a_{DA}$ set to

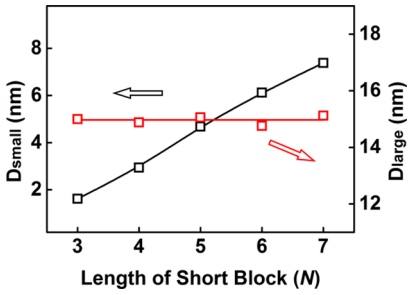


**Figure 7.** Plots of domain size of small and large domains as a function of the length $N$ of the short blocks in the $L_2$-in-L structures self-assembled from $D'_8(A_ND_N)A'_8$ copolymers.

70. As shown in this figure, $L_2$-in-L structures with various sizes of small domains ($D_{small}$) are formed by $D'_8(A_ND_N)A'_8$ multiblock copolymers as the $N$ varies from 3 to 7. In these structures, the domain size of the small domains ($D_{small}$) increases from ~2 to ~8 nm as the length of short blocks increases. The size of large domains ($D_{large}$) remains almost unchanged as $N$ becomes large, which is also shown in Figure 7. To correlate the photovoltaic performance with the size of the small domain, we calculated the photovoltaic properties including $J_{sc}$, PCE, FF, and $V_{oc}$ and plotted them as a function of $D_{small}$. As shown in Figure 8, $V_{oc}$ remains almost unchanged and the FF increases slightly as $D_{small}$ increases. In contrast, $J_{sc}$

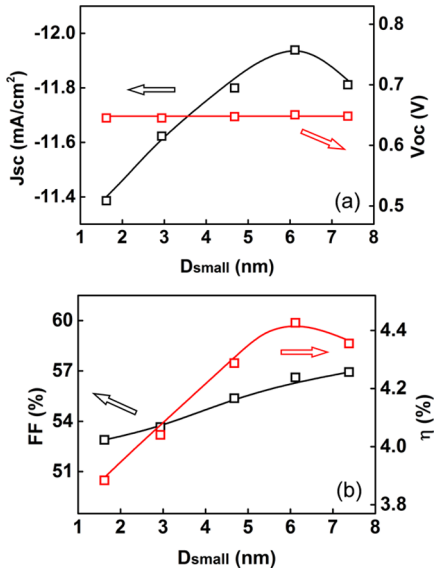


**Figure 8.** Plots of $J_{sc}$ and $V_{oc}$ (a) and FF and $\eta$ (b) as a function of the size of the small domains ($D_{small}$) in the $L_2$-in-L structures self-assembled from $D'_8(A_ND_N)A'_8$ copolymers.

and $\eta$ are significantly affected by the increase in $D_{small}$. Simultaneous increases in $J_{sc}$ and $\eta$ are observed as $D_{small}$ increases from 2 to 6 nm, followed by a decrease, as $D_{small}$ increases from 6 to 8 nm. There is an optimized $D_{small}$ value of 6 nm for the photovoltaic performance. It is worth noting that the $\eta$ of the optimized hierarchical nanostructure is improved by around 25% in comparison with that of general lamellar structures (Figure 3d).

The dependence of $J_{sc}$ on the domain size of hierarchical structures is different from that of general lamellar structures. In general lamellar structures, $J_{sc}$ decreases with increasing domain size, as observed in both experiments and simulations.[35,52,55] In this work, $J_{sc}$ increases with increasing $D_{small}$ when $D_{small}$ is smaller than the optimized domain size. This behavior can be attributed to the fact that small domains promote higher photogenerated current density. In the hierarchical structures, as $D_{small}$ becomes large, the volume fraction of small domains increases, which enhances the photogenerated current density. We compared the photogenerated current density of the hierarchical structures with that of the general lamellar structures (see Figure S5). The photogenerated current density of the hierarchical structures increases with increasing $D_{small}$ when $D_{small} < 6$ nm. In contrast, the photogenerated current density of the general lamella decreases monotonically with increasing domain size. These opposite trends in the dependence of the photogenerated current density on the domain size cause the different trends in the dependence of $J_{sc}$ on the domain size in these two kinds of structures.

As mentioned above, the photovoltaic properties of the hierarchical nanostructures are strongly dependent on the size of the small domains. There is an optimized $D_{small}$ for the highest $J_{sc}$ and $\eta$. In addition, we have calculated the photovoltaic properties of the hierarchical nanostructures with different sizes of the large domains (see Figure S7). The photovoltaic properties decrease as the size of the large domains increases, which is consistent with the experimental observations.[56] However, compared with the effect of the size of the small domains, the size of the large domains has a less


DOI: 10.1021/acsami.8b04692
ACS Appl. Mater. Interfaces 2018, 10, 22552−22561

pronounced effect on the photovoltaic performance of the hierarchical structures. The details of the effect of the size of the large domains on the photovoltaic performance are shown in Section 8 of the Supporting Information.

**2.4. Comparison with Experimental Evidence.** In this subsection, we compare the simulation results with the experimental evidence. Our results demonstrate that hierarchical nanostructures self-assembled from D′(AD)$_n$A′ multiblock copolymers can improve the photovoltaic performance. Some experimental evidence, supporting these simulation results, is available in the literature.[17−20] For example, Yan et al. prepared polymer blend solar cells with hierarchical nanostructures. The polymer solar cells were based on blends of the donor polymer poly(3-hexylthiophene) (P3HT) with the acceptor polymer poly([*N*,*N*′-bis(2-octyldodecyl)-11-naphthalene-1,4,5,8-bis(dicarboximi-de)-2,6-diyl]-*alt*-5,5′-(2,2′-12-bithiophene)) (P(NDI2OD-T2)).[18] It was found that the domain size could be modulated by annealing the samples. The sizes of the small domains in the hierarchical nanostructures evolve from ∼5 to 10 nm with increasing annealing temperature, whereas the larger domains of size ∼100 nm were insensitive to annealing. They examined the photovoltaic properties of these films, and their data are replotted in Figure 9. As shown, $J_{sc}$ peaked at a domain size of

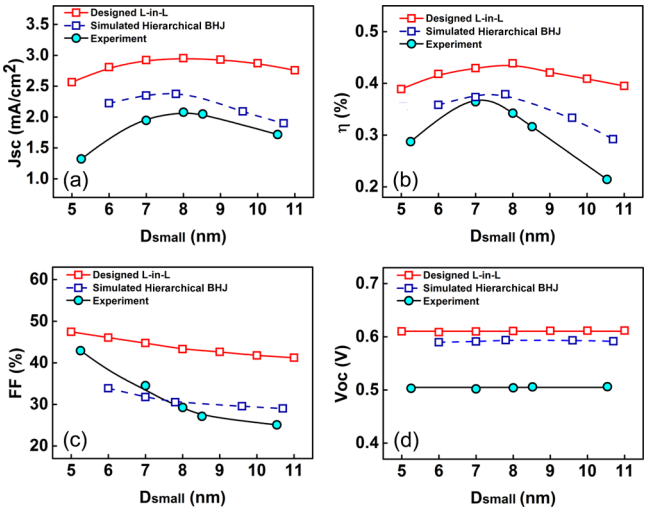


**Figure 9.** Photovoltaic properties including $J_{sc}$ (a), $\eta$ (b), FF (c), and $V_{oc}$ (d) as a function of the size of the small domains in the lamellar-in-lamellar, simulated hierarchical bulk heterojunction (BHJ), and experiments performed by Yan et al. The experimental results in (a−d) were reproduced with permission from ref 18. Copyright 2012, American Chemical Society.

∼8 nm, and the efficiency ($\eta$) was optimized for a domain size of ∼7 nm. Unlike $\eta$ and $J_{sc}$, the FF decreased monotonically with increasing domain size and $V_{oc}$ remained almost unchanged.

The simulation results in the above sections are generally consistent with Yan's experimental observations. We also observed that $J_{sc}$ and $\eta$ increase and $V_{oc}$ remains almost unchanged as the size of the small domains increases (see Figure 8). However, the dependence of FF on $D_{small}$ in the simulation is different from Yan's experimental observations. Whereas the FF increases slightly with increasing $D_{small}$ in our simulation (see Figure 8b), it showed a monotonic decrease in the experiment. The difference between the simulation results shown in Figure 8 and the experimental results probably arises from the difference in the sizes of the large domains. For the nanostructures we considered in Figure 8, the size of the large domain is ∼15 nm. However, in Yan's experiments, the size of the large domain was on the order of 100 nm. Therefore, additional simulations on the photovoltaic properties of hierarchical nanostructures with large domains on the order of 100 nm were needed for comparison with Yan's experimental observations.

In the additional simulations, to make the domain size of the nanostructures comparable to the domain size in Yan's experiments, we designed a model morphology consisting of large domains of 100 nm and small domains varying from 4 to 14 nm. The model morphology was also an **L**-in-**L** hierarchical structure, but the large domains were much larger than those in the hierarchical nanostructures in the above sections. The details of the model morphology are given in the Supporting Information (Figure S8). Because BHJ structures are very different from the designed lamellae-in-lamellae, we simulated a hierarchical BHJ via solving the Cahn−Hilliard equation, which has been widely used to simulate the morphology of polymer blends.[44,47] The mobility parameter in the Cahn−Hilliard equation was set to be space-dependent to obtain hierarchical nanostructures similar to the structures in Yan's experiment, and the values of the other parameters were set according to the literature.[44] Details of the Cahn−Hilliard equation can be found in Section 10 of the Supporting Information. By solving the Cahn−Hilliard equation with space-dependent mobility, we obtained a series of hierarchical BHJ nanostructures with large domain sizes near 100 nm and small domain sizes from ∼6 to ∼11 nm (see Figure S9). Then, we calculated the $J$−$V$ curves of the simulated nanostructures by solving the drift-diffusion equations. The photovoltaic characteristics including $J_{sc}$, $V_{oc}$, FF, and $\eta$ of the designed lamellar-in-lamellae and simulated hierarchical BHJ are plotted in Figure 9. As can be seen, the simulation results, including the photovoltaic properties of the lamellae-in-lamellae and hierarchical BHJ, share the same trend with the experimental results. In the simulations, both $J_{sc}$ and $\eta$ peak at ∼8 nm, whereas $V_{oc}$ remains almost unchanged. For the FF of the simulation results, we observed a steady but slight decrease with increasing $D_{small}$, which was consistent with the experimental observations. Though the performances of the lamellae-in-lamellar and hierarchical BHJ structures share the same trend, the photovoltaic properties of the hierarchical BHJ structures are much more sensitive to the changes in the size of small domains. From the simulated hierarchical BHJ, we can see that the tortuosity and percolation pathways in the BHJ clearly change as the size of the small domain increases, which could significantly affect charge transport and collection, contributing to the high sensitivity of photovoltaic properties to changes in the size of the small domain.

Hierarchical nanostructures, which can enhance the photovoltaic performance of solar cells, can be formed by blending different kinds of polymers. However, from the thermodynamic perspective, the polymer blends tend to form macrophase-separated structures. Though nanostructures can be obtained by increasing the miscibility of blending systems, they are kinetically trapped in a nonequilibrium state.[57,58] It should be emphasized that the long-term morphological stability and controlled miscibility are vital in the field of polymer solar cells. The multiblock copolymers, which can form highly ordered and long-term stable hierarchical nanostructures, can overcome


DOI: 10.1021/acsami.8b04692
ACS Appl. Mater. Interfaces 2018, 10, 22552−22561

the shortcomings noted in the context of blending systems. As a result, materials formed by multiblock copolymers could show advantages in preparing long-term, stable, and high-performance photovoltaics.

In this work, to the best of our knowledge, we provide the first indication that the performance of polymer photovoltaic cells can be improved by the formation of hierarchical nanostructures in designed DA multiblock copolymers. These hierarchical nanostructures display enhanced photovoltaic properties in comparison with general single-periodic nanostructures. The simulation results are found to be in good agreement with the experimental evidence. Additionally, our simulations examine the effects of various parameters, including the number and size of small domains, on the photovoltaic properties. The simulation results provide design guidelines for further improving the photovoltaic performance of hierarchical structures with the number and size of the small domains optimized. Because these morphological characteristics are achievable in multiblock copolymers and can be controlled by the molecular design of the photovoltaic polymers, multiblock copolymers may prove especially attractive in the fabrication of polymer photovoltaic cells.

## 3. CONCLUSIONS

In this work, we utilized a multiscale approach coupling DPD with a drift-diffusion model to investigate the photovoltaic properties of multiblock copolymers in hierarchical **L**-in-**L** structures. The formation of small-length-scale structures in the **L**-in-**L** hierarchical structures yields a significant improvement in photovoltaic performance. We successfully controlled the number and size of small domains in the hierarchical nanostructures by varying the number and length of the short inner blocks, respectively. The optimal number and size of small domains for high power conversion efficiency were obtained via the molecular design of multiblock copolymers. The high power conversion efficiency is a result of the balance among the generation, recombination, and transport of charge carriers. The improvement in the photovoltaic properties in the hierarchical nanostructures is in qualitative agreement with recent experimental evidence. Our simulation results could provide useful information for preparing photovoltaic devices with enhanced performance through designing and controlling the hierarchical nanostructures.

## 4. METHODS

To correlate the relationship between the self-assembled morphologies and the photovoltaic properties of the multiblock copolymers, we coupled the DPD method with a drift-diffusion model. The DPD method was conducted for morphology studies, and then the drift-diffusion equations were solved for calculations of photovoltaic properties.

Mesoscopic simulations based on the DPD are performed to investigate the self-assembled morphologies.[59−63] DPD is a powerful tool that can be used for modelling physical phenomena occurring on larger time and length scales than typical molecular dynamics. In the DPD method, a coarse graining bead (DPD bead) represents a cluster of atoms. The evolution of the DPD beads is described by Newton's equations of motion. Newton's equations of motion for all bead positions and velocities are integrated by a modified velocity-Verlet algorithm. The force acting on a DPD bead $\alpha$, $\mathbf{f}_\alpha$, includes the conservative force ($\mathbf{F}^{C}_{\alpha\beta}$), dissipative force ($\mathbf{F}^{D}_{\alpha\beta}$), and random force ($\mathbf{F}^{R}_{\alpha\beta}$). It is given by[51]

$$\mathbf{f}_\alpha = \sum_{\beta\neq\alpha} (\mathbf{F}^{C}_{\alpha\beta} + \mathbf{F}^{D}_{\alpha\beta} + \mathbf{F}^{R}_{\alpha\beta}) \quad (1)$$

More details of the DPD simulation method can be found in Section 1 of the Supporting Information.

In the DPD simulations, we consider a series of donor−acceptor multiblock copolymers consisting of short and long blocks. The neighboring beads in each copolymer are connected by bonds. The bonds are represented by a harmonic spring potential,

$$U_{\alpha\beta} = K_b(1 - r_{\alpha\beta}/r_{eq})^2 \quad (2)$$

where the spring constant and the equilibrium bond distance are set to $K_b = 50$ and $r_{eq} = 0.5$, respectively. Because most semiconductor polymers are rigid, we include a three-body stiffness potential along the copolymer with the form

$$U_{angle} = K_a(\cos\theta - \cos\theta_0)^2 \quad (3)$$

where $K_a = 15$ and $\theta_0 = \pi$.

All DPD simulations are performed in a $32 \times 32 \times 32$ simulation box, where NVT ensemble and periodic boundary conditions are adopted. The particle density $\rho$ is set to 3. The interaction strengths $a_{ij}$ between DPD beads of same type are given by $a_{DD} = a_{AA} = 25$, where D and A stand for the beads in the donor and acceptor blocks, respectively. The friction coefficient $\gamma$ and the noise amplitude $\sigma$ are, respectively, set to 4.5 and 3.0, and thus $k_BT = 1.0$. In this work, more than $2 \times 10^7$ DPD steps are performed so that the computing time is long enough for the system to achieve an equilibrium state. To establish a correlation between simulation parameters and experimental values and thus establish a physical length scale in our system, we equate the thickness of a lamellar layer obtained from DPD for the $D_8A_8$ donor−acceptor diblock to 15 nm.[9] These layers are then sandwiched between two electrodes with the lamellar domains perpendicular to the electrodes.

After obtaining the self-assembled morphologies by DPD simulation, we calculate the photovoltaic properties of these morphologies by solving the drift-diffusion equations involving the electric potential $\psi$ (V) and the charge carrier number densities $e$, $h$, and $X$ ($m^{-3}$) of electrons, holes, and excitons. The current densities of the holes and electrons are calculated using the forms[64]

$$\mathbf{J}_e = -\mu_e(\mathbf{r})e(\mathbf{r})\nabla\psi(\mathbf{r}) - D_e(\mathbf{r})\nabla e(\mathbf{r}) \quad (4)$$

$$\mathbf{J}_h = \mu_h(\mathbf{r})h(\mathbf{r})\nabla\psi(\mathbf{r}) - D_h(\mathbf{r})\nabla h(\mathbf{r}) \quad (5)$$

The total current density $\mathbf{J}$ is the summation of $\mathbf{J}_e$ and $\mathbf{J}_h$. More details of the drift-diffusion model are shown in Section 2 of the Supporting Information. The drift-diffusion equations in the drift-diffusion model are numerically solved by the finite difference method.

The output of the DPD simulations serves as the input to estimate the local dielectric constants and mobility constants at the center of mesh cells in the finite difference method for the drift-diffusion equations. The total dielectric constants $\varepsilon(\mathbf{r})$ and mobility constants $\mu(\mathbf{r})$ at each point are obtained by linearly weighting the contributions of the different components based on the respective volume fractions, i.e.,

$$\varepsilon(\mathbf{r}) = \sum_i \varphi_i(\mathbf{r})\varepsilon_i \quad (6)$$

$$\mu(\mathbf{r}) = \sum_i \varphi_i(\mathbf{r})\mu_i \quad (7)$$

where $\varepsilon_i$ and $\mu_i$ denote the permittivity and mobility constants of component $i$, respectively, and $\varphi_i(\mathbf{r})$ refers to the volume fraction of component $i$ at $\mathbf{r}$.



DOI: 10.1021/acsami.8b04692
ACS Appl. Mater. Interfaces 2018, 10, 22552−22561

## ■ ASSOCIATED CONTENT

### Supporting Information

The Supporting Information is available free of charge on the ACS Publications website at DOI: 10.1021/acsami.8b04692.

Details of simulation methods; comparison between lamellae-in-lamellar and optimized lamellar structures; photovoltaic performance for hierarchical nanostructures with high mobility and short exciton lifetime; photogenerated and recombination current densities; effect of size of large-length-scale domains on photovoltaic properties; model morphology; and simulated hierarchical BHJ (PDF)

## ■ AUTHOR INFORMATION


### Corresponding Authors

*E-mail: jlin@ecust.edu.cn (J.L.).
*E-mail: lq_wang@ecust.edu.cn (L.W.).

### ORCID

Jiaping Lin: 0000-0001-9633-4483
Liangshun Zhang: 0000-0002-0182-7486
Gengchao Wang: 0000-0002-5421-0164


### Notes

The authors declare no competing financial interest.

## ■ ACKNOWLEDGMENTS

This work was supported by the National Natural Science Foundation of China (21774032, 21474029, and 51621002). Support from Project of Shanghai Municipality (16520721900 and 14DZ2261205) is also appreciated.

## ■ REFERENCES


(1) Zhao, K.; Hu, H.; Spada, E.; Jagadamma, L. K.; Yan, B.; Abdelsamie, M.; Yang, Y.; Yu, L.; Munir, R.; Li, R.; Ndjawa, G. O. N.; Amassian, A. Highly Efficient Polymer Solar Cells with Printed Photoactive Layer: Rational Process Transfer from Spin-Coating. *J. Mater. Chem. A* **2016**, *4*, 16036−16046.

(2) Günes, S.; Neugebauer, H.; Sariciftci, N. S. Conjugated Polymer-Based Organic Solar Cells. *Chem. Rev.* **2007**, *107*, 1324−1338.

(3) Li, G.; Zhu, R.; Yang, Y. Polymer Solar Cells. *Nat. Photonics* **2012**, *6*, 153−161.

(4) Polman, A.; Knight, M.; Garnett, E. C.; Ehrler, B.; Sinke, W. C. Photovoltaic Materials: Present Efficiencies and Future Challenges. *Science* **2016**, *352*, aad4424.

(5) Zhao, W.; Qian, D.; Zhang, S.; Li, S.; Inganäs, O.; Gao, F.; Hou, J. Fullerene-Free Polymer Solar Cells with over 11% Efficiency and Excellent Thermal Stability. *Adv. Mater.* **2016**, *28*, 4734−4739.

(6) Li, M.; Gao, K.; Wan, X.; Zhang, Q.; Kan, B.; Xia, R.; Liu, F.; Yang, X.; Feng, H.; Ni, W.; Wang, Y.; Peng, J.; Zhang, H.; Liang, Z.; Yip, H.-L.; Peng, X.; Cao, Y.; Chen, Y. Solution-Processed Organic Tandem Solar Cells with Power Conversion Efficiencies >12%. *Nat. Photonics* **2017**, *11*, 85−90.

(7) Li, N.; Brabec, C. J. Air-Processed Polymer Tandem Solar Cells with Power Conversion Efficiency Exceeding 10%. *Energy Environ. Sci.* **2015**, *8*, 2902−2909.

(8) Chen, S.; Cho, H. J.; Lee, J.; Yang, Y.; Zhang, Z.-G.; Li, Y.; Yang, C. Modulating the Molecular Packing and Nanophase Blending Via a Random Terpolymerization Strategy toward 11% Efficiency Non-fullerene Polymer Solar Cells. *Adv. Energy Mater.* **2017**, *7*, 1701125.

(9) Guo, C.; Lin, Y.-H.; Witman, M. D.; Smith, K. A.; Wang, C.; Hexemer, A.; Strzalka, J.; Gomez, E. D.; Verduzco, R. Conjugated Block Copolymer Photovoltaics with near 3% Efficiency through Microphase Separation. *Nano Lett.* **2013**, *13*, 2957−2963.

(10) Mitchell, V. D.; Jones, D. J. Advances Towards the Effective Use of Block Copolymers as Organic Photovoltaic Active Layers. *Polym. Chem.* **2018**, *9*, 795.

(11) Gieseking, B.; Jäck, B.; Preis, E.; Jung, S.; Forster, M.; Scherf, U.; Deibel, C.; Dyakonov, V. Excitation Dynamics in Low Band Gap Donor-Acceptor Copolymers and Blends. *Adv. Energy Mater.* **2012**, *2*, 1477−1482.

(12) Zhou, N.; Lin, H.; Lou, S. J.; Yu, X.; Guo, P.; Manley, E. F.; Loser, S.; Hartnett, P.; Huang, H.; Wasielewski, M. R.; Chen, L. X.; Chang, R. P. H.; Facchetti, A.; Marks, T. J. Morphology-Performance Relationships in High-Efficiency All-Polymer Solar Cells. *Adv. Energy Mater.* **2014**, *4*, 1300785.

(13) Benten, H.; Mori, D.; Ohkita, H.; Ito, S. Recent Research Progress of Polymer Donor/Polymer Acceptor Blend Solar Cells. *J. Mater. Chem. A* **2016**, *4*, 5340−5365.

(14) Yang, Y.; Mielczarek, K.; Aryal, M.; Zakhidov, A.; Hu, W. Effects of Nanostructure Geometry on Nanoimprinted Polymer Photovoltaics. *Nanoscale* **2014**, *6*, 7576−7584.

(15) Yang, Y.; Mielczarek, K.; Aryal, M.; Zakhidov, A.; Hu, W. Nanoimprinted Polymer Solar Cell. *ACS Nano* **2012**, *6*, 2877−2892.

(16) Kimber, R. G. E.; Walker, A. B.; Schröder-Turk, G. E.; Cleaver, D. J. Bicontinuous Minimal Surface Nanostructures for Polymer Blend Solar Cells. *Phys. Chem. Chem. Phys.* **2010**, *12*, 844−851.

(17) Chen, W.; Xu, T.; He, F.; Wang, W.; Wang, C.; Strzalka, J.; Liu, Y.; Wen, J.; Miller, D. J.; Chen, J.; Hong, K.; Yu, L.; Darling, S. B. Hierarchical Nanomorphologies Promote Exciton Dissociation in Polymer/Fullerene Bulk Heterojunction Solar Cells. *Nano Lett.* **2011**, *11*, 3707−3713.

(18) Yan, H.; Collins, B. A.; Gann, E.; Wang, C.; Ade, H.; McNeill, C. R. Correlating the Efficiency and Nanomorphology of Polymer Blend Solar Cells Utilizing Resonant Soft X-Ray Scattering. *ACS Nano* **2012**, *6*, 677−688.

(19) Huang, Y.-C.; Tsao, C.-S.; Huang, T.-Y.; Cha, H.-C.; Patra, D.; Su, C.-J.; Jeng, U.-S.; Ho, K.-C.; Wei, K.-H.; Chu, C.-W. Quantitative Characterization and Mechanism of Formation of Multilength-Scale Bulk Heterojunction Structures in Highly Efficient Solution-Processed Small-Molecule Organic Solar Cells. *J. Phys. Chem. C* **2015**, *119*, 16507−16517.

(20) Fang, J.; Wang, Z.; Zhang, J.; Zhang, Y.; Deng, D.; Wang, Z.; Lu, K.; Ma, W.; Wei, Z. Understanding the Impact of Hierarchical Nanostructure in Ternary Organic Solar Cells. *Adv. Sci.* **2015**, *2*, 1500250.

(21) Lee, Y.; Gomez, E. D. Challenges and Opportunities in the Development of Conjugated Block Copolymers for Photovoltaics. *Macromolecules* **2015**, *48*, 7385−7395.

(22) He, M.; Qiu, F.; Lin, Z. Conjugated Rod-Coil and Rod-Rod Block Copolymers for Photovoltaic Applications. *J. Mater. Chem.* **2011**, *21*, 17039−17048.

(23) ten Brinke, G.; Loos, K.; Vukovic, I.; du Sart, G. G. Hierarchical Self-Assembly of Two-Length-Scale Multiblock Copolymers. *J. Phys.: Condens. Matter* **2011**, *23*, 284110.

(24) Wang, L.; Lin, J.; Zhang, X. Hierarchical Microstructures Self-Assembled from Polymer Systems. *Polymer* **2013**, *54*, 3427−3442.

(25) Tung, S.-H.; Kalarickal, N. C.; Mays, J. W.; Xu, T. Hierarchical Assemblies of Block-Copolymer-Based Supramolecules in Thin Films. *Macromolecules* **2008**, *41*, 6453−6462.

(26) Masuda, J.; Takano, A.; Nagata, Y.; Noro, A.; Matsushita, Y. Nanophase-Separated Synchronizing Structure with Parallel Double Periodicity from an Undecablock Terpolymer. *Phys. Rev. Lett.* **2006**, *97*, 098301.

(27) Faber, M.; Voet, V. S. D.; ten Brinke, G.; Loos, K. Preparation and Self-Assembly of Two-Length-Scale A-b-$(B\text{-}b\text{-}A)_n$-b-B Multiblock Copolymers. *Soft Matter* **2012**, *8*, 4479−4485.

(28) Wang, L.; Lin, J.; Zhang, L. Hierarchically Ordered Microstructures Self-Assembled from $A(BC)_n$ Multiblock Copolymers. *Macromolecules* **2010**, *43*, 1602−1609.

(29) Zhang, X.; Wang, L.; Zhang, L.; Lin, J.; Jiang, T. Controllable Hierarchical Microstructures Self-Assembled from Multiblock Copolymers Confined in Thin Films. *Langmuir* **2015**, *31*, 2533−2544.




DOI: 10.1021/acsami.8b04692
ACS Appl. Mater. Interfaces 2018, 10, 22552−22561

(30) Zhu, X.; Wang, L.; Lin, J. Distinct Elastic Response to Hierarchical Nanostructures. *Macromolecules* **2011**, *44*, 8314−8323.
(31) Nakabayashi, K.; Mori, H. All-Polymer Solar Cells Based on Fully Conjugated Block Copolymers Composed of Poly(3-Hexylthiophene) and Poly(Naphthalene Bisimide) Segments. *Macromolecules* **2012**, *45*, 9618−9625.
(32) Wang, S.; Yang, Q.; Tao, Y.; Guo, Y.; Yang, J.; Liu, Y.; Zhao, L.; Xie, Z.; Huang, W. Fully Conjugated Block Copolymers for Single-Component Solar Cells: Synthesis, Purification, and Characterization. *New J. Chem.* **2016**, *40*, 1825−1833.
(33) Hiorns, R. C.; Cloutet, E.; Ibarboure, E.; Khoukh, A.; Bejbouji, H.; Vignau, L.; Cramail, H. Synthesis of Donor-Acceptor Multiblock Copolymers Incorporating Fullerene Backbone Repeat Units. *Macromolecules* **2010**, *43*, 6033−6044.
(34) Root, S. E.; Jackson, N. E.; Savagatrup, S.; Arya, G.; Lipomi, D. J. Modelling the Morphology and Thermomechanical Behaviour of Low-Bandgap Conjugated Polymers and Bulk Heterojunction Films. *Energy Environ. Sci.* **2017**, *10*, 558−569.
(35) Shah, M.; Ganesan, V. Correlations between Morphologies and Photovoltaic Properties of Rod-Coil Block Copolymers. *Macromolecules* **2010**, *43*, 543−552.
(36) Neupane, U.; Bahrami, B.; Biesecker, M.; Baroughi, M. F.; Qiao, Q. Kinetic Monte Carlo Modeling on Organic Solar Cells: Domain Size, Donor-Acceptor Ratio and Thickness. *Nano Energy* **2017**, *35*, 128−137.
(37) Min Nam, Y.; Huh, J.; Ho Jo, W. Optimization of Thickness and Morphology of Active Layer for High Performance of Bulk-Heterojunction Organic Solar Cells. *Sol. Energy Mater. Sol. Cells* **2010**, *94*, 1118−1124.
(38) Bartesaghi, D.; van der Kaap, N.; Koster, L. J. A. 3D Simulations of Organic Solar Cells. *Unconventional Thin Film Photovoltaics*, 2016; pp 420−452.
(39) Groves, C. Developing Understanding of Organic Photovoltaic Devices: Kinetic Monte Carlo Models of Geminate and Non-Geminate Recombination, Charge Transport and Charge Extraction. *Energy Environ. Sci.* **2013**, *6*, 3202−3217.
(40) Koster, L. J. A.; Stenzel, O.; Oosterhout, S. D.; Wienk, M. M.; Schmidt, V.; Janssen, R. A. J. Morphology and Efficiency: the Case of Polymer/ZnO Solar Cells. *Adv. Energy Mater.* **2013**, *3*, 615−621.
(41) Hufnagel, M.; Fischer, M.; Thurn-Albrecht, T.; Thelakkat, M. Influence of Fullerene Grafting Density on Structure, Dynamics, and Charge Transport in P3HT-b-PPC$_{61}$BM Block Copolymers. *Macromolecules* **2016**, *49*, 1637−1647.
(42) Koster, L. J. A.; Smits, E. C. P.; Mihailetchi, V. D.; Blom, P. W. M. Device Model for The Operation of Polymer/Fullerene Bulk Heterojunction Solar Cells. *Phys. Rev. B: Condens. Matter Mater. Phys.* **2005**, *72*, 085205.
(43) Buxton, G. A.; Clarke, N. Computer Simulation of Polymer Solar Cells. *Modell. Simul. Mater. Sci. Eng.* **2007**, *15*, 13.
(44) Ray, B.; Nair, P. R.; Alam, M. A. Annealing Dependent Performance of Organic Bulk-Heterojunction Solar Cells: A Theoretical Perspective. *Sol. Energy Mater. Sol. Cells* **2011**, *95*, 3287−3294.
(45) McNeill, C. R.; Westenhoff, S.; Groves, C.; Friend, R. H.; Greenham, N. C. Influence of Nanoscale Phase Separation on the Charge Generation Dynamics and Photovoltaic Performance of Conjugated Polymer Blends: Balancing Charge Generation and Separation. *J. Phys. Chem. C* **2007**, *111*, 19153−19160.
(46) Ye, L.; Hu, H.; Ghasemi, M.; Wang, T.; Collins, B. A.; Kim, J.-H.; Jiang, K.; Carpenter, J. H.; Li, H.; Li, Z.; McAfee, T. Quantitative Relations between Interaction Parameter, Miscibility and Function in Organic Solar Cells. *Nat. Mater.* **2018**, *17*, 253.
(47) Lyons, B. P.; Clarke, N.; Groves, C. The Relative Importance of Domain Size, Domain Purity and Domain Interfaces to the Performance of Bulk-Heterojunction Organic Photovoltaics. *Energy Environ. Sci.* **2012**, *5*, 7657−7663.
(48) Burke, T. M.; McGehee, M. D. How High Local Charge Carrier Mobility and an Energy Cascade in a Three-Phase Bulk Heterojunction Enable >90% Quantum Efficiency. *Adv. Mater.* **2014**, *26*, 1923−1928.
(49) Sweetnam, S.; Graham, K. R.; Ngongang Ndjawa, G. O.; Heumüller, T.; Bartelt, J. A.; Burke, T. M.; Li, W.; You, W.; Amassian, A.; McGehee, M. D. Characterization of the Polymer Energy Landscape in Polymer:Fullerene Bulk Heterojunctions with Pure and Mixed Phases. *J. Am. Chem. Soc.* **2014**, *136*, 14078−14088.
(50) Burke, T. M.; Sweetnam, S.; Vandewal, K.; McGehee, M. D. Beyond Langevin Recombination: How Equilibrium between Free Carriers and Charge Transfer States Determines the Open-Circuit Voltage of Organic Solar Cells. Adv. *Energy Mater* **2015**, *5*, 1500123.
(51) Zhu, X.; Wang, L.; Lin, J. Self-Assembly of Rod-Coil Multiblock Copolymers: A Strategy for Creating Hierarchical Smectic Structures. *J. Phys. Chem. B* **2013**, *117*, 5748−5756.
(52) Lee, C.; Li, Y.; Lee, W.; Lee, Y.; Choi, J.; Kim, T.; Wang, C.; Gomez, E. D.; Woo, H. Y.; Kim, B. J. Correlation between Phase-Separated Domain Sizes of Active Layer and Photovoltaic Performances in All-Polymer Solar Cells. *Macromolecules* **2016**, *49*, 5051−5058.
(53) Tao, Y.; Ma, B.; Segalman, R. A. Self-Assembly of Rod-Coil Block Copolymers and Their Application in Electroluminescent Devices. *Macromolecules* **2008**, *41*, 7152−7159.
(54) Sommer, M.; Huettner, S.; Thelakkat, M. Donor-Acceptor Block Copolymers for Photovoltaic Applications. *J. Mater. Chem.* **2010**, *20*, 10788−10797.
(55) Buxton, G. A.; Clarke, N. Computer Simulation of Polymer Solar Cells. *Modell. Simul. Mater. Sci. Eng.* **2007**, *15*, 13.
(56) Ye, L.; Xiong, Y.; Li, S.; Ghasemi, M.; Balar, N.; Turner, J.; Gadisa, A.; Hou, J.; O'Connor, B. T.; Ade, H. Precise Manipulation of Multilength Scale Morphology and Its Influence on Eco-Friendly Printed All-Polymer Solar Cells. *Adv. Funct. Mater.* **2017**, *27*, 1702016.
(57) Li, N.; Perea, J. D.; Kassar, T.; Richter, M.; Heumueller, T.; Matt, G. J.; Hou, Y.; Güldal, N. S.; Chen, H.; Chen, S.; Langner, S.; Berlinghof, M.; Unruh, T.; Brabec, C. J. Abnormal strong burn-in degradation of highly efficient polymer solar cells caused by spinodal donor-acceptor demixing. *Nat. Commun.* **2017**, *8*, 14541.
(58) Ghasemi, M.; Ye, L.; Zhang, Q.; Yan, L.; Kim, J.-H.; Awartani, O.; You, W.; Gadisa, A.; Ade, H. Panchromatic Sequentially Cast Ternary Polymer Solar Cells. *Adv. Mater.* **2017**, *29*, 1604603.
(59) Groot, R. D.; Madden, T. J. Dynamic Simulation of Diblock Copolymer Microphase Separation. *J. Chem. Phys.* **1998**, *108*, 8713−8724.
(60) Groot, R. D.; Warren, P. B. Dissipative Particle Dynamics: Bridging the Gap between Atomistic and Mesoscopic Simulation. *J. Chem. Phys.* **1997**, *107*, 4423−4435.
(61) Xu, Z.; Lin, J.; Zhang, Q.; Wang, L.; Tian, X. Theoretical Simulations of Nanostructures Self-Assembled from Copolymer Systems. *Polym. Chem.* **2016**, *7*, 3783−3811.
(62) Zhang, Q.; Lin, J.; Wang, L.; Xu, Z. Theoretical Modeling and Simulations of Self-Assembly of Copolymers in Solution. *Prog. Polym. Sci.* **2017**, *75*, 1−30.
(63) Dong, B.; Huang, Z.; Chen, H.; Yan, L.-T. Chain-Stiffness-Induced Entropy Effects Mediate Interfacial Assembly of Janus Nanoparticles in Block Copolymers: From Interfacial Nanostructures to Optical Responses. *Macromolecules* **2015**, *48*, 5385−5393.
(64) Monestier, F.; Simon, J.-J.; Torchio, P.; Escoubas, L.; Flory, F.; Bailly, S.; de Bettignies, R.; Guillerez, S.; Defranoux, C. Modeling the Short-Circuit Current Density of Polymer Solar Cells Based on P3HT: PCBM Blend. *Sol. Energy Mater. Sol. Cells* **2007**, *91*, 405−410.


DOI: 10.1021/acsami.8b04692
*ACS Appl. Mater. Interfaces* 2018, 10, 22552−22561